Nonlinear current response of one- and two-band superconductors

E. J. Nicol*
Department of Physics, University of Guelph, Guelph, Ontario, Canada N1G 2W1

J. P. Carbotte†
Department of Physics and Astronomy, McMaster University, Hamilton, Ontario, Canada L8S 4M1

D. J. Scalapino‡
Department of Physics, University of California, Santa Barbara, California, 93106-9530, USA
(Received 7 October 2005; published 24 January 2006)

We have calculated the nonlinear current of a number of single band *s*-wave electron-phonon superconductors. Among issues considered were those of dimensionality, strong electron-phonon coupling, impurities, and comparison with BCS. For the case of two bands, particular attention is paid to features resulting from the two energy gap scales, the Fermi velocity anisotropy, the integration effects of the off-diagonal electron-phonon interaction, as well as interband and intraband impurities. For the specific case of MgB_2, we present results based on the known microscopic parameters of band theory.

DOI: 10.1103/PhysRevB.73.014521 PACS number(s): 74.20.−z, 74.70.Ad, 74.25.Fy

I. INTRODUCTION

With the advent of high temperature superconductivity in the cuprates and the possibility of exotic gap symmetry including nodal behavior, a renewed effort to find experimental probes of order parameter symmetry has ensued. One result of this effort was the proposal by Sauls and co-workers[1,2] to examine the nonlinear current response of *d*-wave superconductors. They showed that a nonanalyticity in the current-velocity relation at temperature $T=0$ is introduced by the presence of nodes in the order parameter. One prediction was that an anisotropy should exist in the nonlinear current as a function of the direction of the superfluid velocity relative to the position of the node. This would be reflected in an anisotropy of a term in the inverse penetration depth which is linear in the magnetic field H. Early experimental work did not verify these predictions[3] and it was suggested that impurity scattering[2] or nonlocal effects[4] may be responsible. However, a more recent reanalysis of experiment has claimed to confirm the predictions.[5] An alternative proposal was given by Dahm and Scalapino[6] who examined the quadratic term in the magnetic response of the penetration depth, which shows a $1/T$ dependence at low T as first discussed by Xu *et al.*[2] Dahm and Scalapino demonstrated that this upturn would provide a clear and unique signature of the nodes in the *d*-wave gap and that this feature could be measured directly via microwave intermodulation effects. Indeed, experimental verification of this has been obtained[7] confirming that nonlinear microwave current response can be used as a sensitive probe of issues associated with the order parameter symmetry. Thus, we are led to consider further cases of gap anisotropy and turn our attention to the two-band superconductor MgB_2 which is already under scrutiny for possible applications, including passive microwave filter technology.[8] MgB_2 was discovered in 2001 (Ref. 9) and since this time an enormous scientific effort has focused on this material. On the basis of the evidence that is available, it is now thought that this material may be our best candidate for a classic two-band electron-phonon superconductor, with *s*-wave pairing in each channel.[10] A heightened interest in two-band superconductivity has led to claims of possible two-band effects in many other materials, both old[11] and new.[12]

Our goal is to compare in detail the differences between one-band and two-band *s*-wave superconductors in terms of their nonlinear response, that would be measured in the coefficients defined by Xu *et al.*[2] and Dahm and Scalapino.[13] This leads us to reconsider the one-band *s*-wave case, where we study issues of dimensionality, impurities, and strong electron-phonon coupling. We find new effects due to strong coupling at both high and low T. We then examine the situation for two-band superconductors, starting from a case of highly decoupled bands. Here, we are looking for signatures of the low energy scale due to the smaller gap, the effect of integration of the bands, and the response to interband and intraband impurities. Unusual behavior exists distinctly different from the one-band case and not necessarily understood as a superposition of two separate superconductors. Finally, we return to the case of MgB_2 which was studied previously via a more approximate approach.[13] In the current work, we are able to use the complete microscopic theory with the parameters and the electron-phonon spectral functions taken from band structure.[10,14] In this way, we provide more detailed predictions for the nonlinear coefficient of MgB_2.

In Sec. II, we briefly summarize the necessary theory for calculating the gap and renormalization function in two-band superconductors, from which the current as a function of the superfluid velocity v_s is then derived. In Sec. III, we explain our procedure for extracting the temperature-dependent nonlinear term from the current and we examine the characteristic features for one-band superconductors in light of issues of dimensionality, impurity scattering and strong coupling. Section IV presents the results of two-band superconductors and simple formulas are given for limiting cases which aid in illuminating the effects of gap and Fermi velocity anisotropy. The case of MgB_2 is also discussed. We form our conclusions in Sec. V.

II. THEORY

The superfluid current has been considered theoretically in the past by many authors for s-wave[15–22] and for other order parameters, such as d-wave and f-wave.[1,2,23–25] Most recently, the case of two-band superconductivity has been examined[13,26,27] with good agreement obtained between theory and experiment for the temperature dependence of the critical current.[26]

In this work, we wish to calculate the superfluid current as a function of superfluid velocity v_s or momentum q_s and extract from this the nonlinear term. To do this, we choose to evaluate the expression for the superfluid current density j_s that is written on the imaginary axis in terms of Matsubara quantities.[19,26] This naturally allows for the inclusion of impurity scattering and strong electron-phonon coupling in a numerically efficient manner. Written in general for two-bands having a current j_{s1} and j_{s2}, for the first and second band, respectively, we have

$$j_s = \sum_{l=1}^{2} \frac{3en_l}{mv_{Fl}} \pi T \sum_{n=-\infty}^{+\infty} \left\langle \frac{i[\tilde{\omega}_l(n) - is_l z]z}{\sqrt{[\tilde{\omega}_l(n) - is_l z]^2 + \tilde{\Delta}_l^2(n)}} \right\rangle_l, \quad (1)$$

where e is the electric charge, m is the electron mass, T is the temperature, $s_l = v_{Fl} q_s$, n_l is the electron density, and v_{Fl} is the Fermi velocity of the lth band ($l=1,2$). The $\langle \cdots \rangle_l$ represents an integration for the lth band which is given as $\int_{-1}^{1} dz/2$ for a $3d$ band and $\int_0^{2\pi} d\theta/(2\pi)$ for a $2d$ band, with $z=\cos\theta$ in the $2d$ case. Also, in the expression for the current, the 3 should be changed to a 2 for $2d$. This is done within a mean-field treatment and ignoring critical fluctuations near T_c. Here, we have taken the approximation of a spherical Fermi surface in $3d$ and a cylindrical one in $2d$ as we will see further on that the differences between $2d$ and $3d$ are not significant to more than a overall numerical factor and so providing more precise Fermi surface averages will not change the results in a meaningful way. To evaluate this expression, we require the solution of the standard s-wave Eliashberg equations for the renormalized gaps and frequencies $\tilde{\Delta}_l(n) = Z_l(n)\Delta_l(n)$ and $\tilde{\omega}_l(n) = Z_l(n)\omega_n$, respectively. These have been generalized to two bands and must also include the effect of the current through q_s. With further details given in Refs. 10 and 22 we merely state them here

$$\tilde{\Delta}_l(n) = \pi T \sum_m \sum_j [\lambda_{lj}(m-n) - \mu_{lj}^*(\omega_c)\theta(\omega_c - |\omega_m|)] \times \left\langle \frac{\tilde{\Delta}_j(m)}{\sqrt{[\tilde{\omega}_j(m) - is_j z]^2 + \tilde{\Delta}_j^2(m)}} \right\rangle_j + \pi \sum_j t_{lj}^+ \left\langle \frac{\tilde{\Delta}_j(n)}{\sqrt{[\tilde{\omega}_j(n) - is_j z]^2 + \tilde{\Delta}_j^2(n)}} \right\rangle_j \quad (2)$$

and

$$\tilde{\omega}_l(n) = \omega_n + \pi T \sum_m \sum_j \lambda_{lj}(m-n) \times \left\langle \frac{\tilde{\omega}_j(m) - is_j z}{\sqrt{[\tilde{\omega}_j(m) - is_j z]^2 + \tilde{\Delta}_j^2(m)}} \right\rangle_j + \pi \sum_j t_{lj}^+ \left\langle \frac{\tilde{\omega}_j(n) - is_j z}{\sqrt{[\tilde{\omega}_j(n) - is_j z]^2 + \tilde{\Delta}_j^2(n)}} \right\rangle_j, \quad (3)$$

where j sums over the number of bands and the sum over m is from $-\infty$ to ∞. Here, $t_{lj}^+ = 1/(2\pi\tau_{lj}^+)$ is the ordinary impurity scattering rate and n indexes the nth Matsubara frequency ω_n, with $\omega_n = (2n-1)\pi T$, where $n = 0, \pm 1, \pm 2, \ldots$. The μ_{lj}^* are Coulomb repulsions, which require a high energy cutoff ω_c, taken to be about 6 to 10 times the maximum phonon frequency, and the electron-phonon interaction enters through

$$\lambda_{lj}(m-n) \equiv 2\int_0^\infty \frac{\Omega \alpha^2 F_{lj}(\Omega)}{\Omega^2 + (\omega_n - \omega_m)^2} d\Omega \quad (4)$$

with $\alpha_{lj}^2 F(\Omega)$ the electron-phonon spectral functions and Ω the phonon energy. Note that the dimensionality does not change the gap equations when there is no current. For finite q_s, it does and we will see later the result of this effect. Likewise, an essential ingredient is that the current enters the Eliashberg equations and provides the bulk of the nonlinear effect for temperatures above $T \sim 0.5T_c$. Indeed, at T_c all of the nonlinearity arises from the gap.

We now proceed to the case of one-band superconductors, to illustrate the generic features of the superfluid current and demonstrate how we extract the nonlinear term. In the section following, we will return to the two-band case.

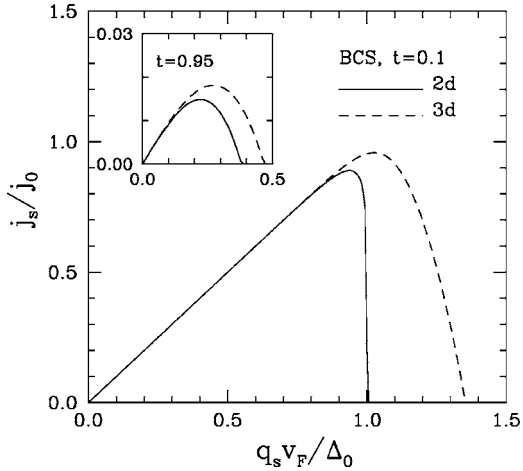

FIG. 1. The normalized current j_s/j_0 as a function of $q_s v_F/\Delta_0$, where $j_0 = ne\Delta_0/(mv_F)$ and Δ_0 is the energy gap at $T=0$. Shown are the low temperature BCS curves for two dimensions (solid line) and three dimensions (dashed line), given for a reduced temperature $t=T/T_c=0.1$. The inset is for near T_c at $t=0.95$.

III. ONE-BAND *s*-WAVE SUPERCONDUCTORS

In Fig. 1, we illustrate that these equations reproduce the standard results for j_s versus q_s for a one-band superconductor in the weak-coupling BCS limit. Equations (1)–(3) were solved for both the $2d$ and $3d$ cases at $t=T/T_c=0.1$ and 0.95. The $T=0$ result of past literature[15,16,19] is recovered in the case of $3d$. One sees for $t=0.1$ at low q_s, the curve is essentially linear, reflecting the relationship of $j_s=n_s e v_s$, with n_s the superfluid density. For strong coupling, the slope would be reduced by approximately $1+\lambda$ as the superfluid condensate is also reduced by this factor. Likewise the reduction in the slope with temperature would reflect the temperature dependence of the superfluid density. Indeed, to provide these curves using the Eliashberg equations, we used the $\alpha^2F(\omega)$ spectrum of Al and made the corrections for the $1+\lambda$ factor. Al is a classic BCS weak-coupling superconductor, that agrees with BCS in every way and is generally used for BCS tests of the Eliashberg equations. The λ for Al is 0.43. While at low T the curves show little deviation from linearity at low q_s, and thus the nonlinear correction will be essentially zero (exponentially so with temperature in BCS theory), at T near T_c, one sees that there is more curvature for $q_s \to 0$ and hence a larger nonlinear term is expected. However, while the $2d$ and $3d$ curves differ in behavior near the maximum in j_s, one finds that the behavior at low q_s is very similar. Indeed, the nonlinearity is a very small effect on these plots and hard to discern, however, it will be borne out in our paper that the nonlinear current does not show significant differences in the T-dependence between $2d$ and $3d$. Nevertheless, we will still include both the $2d$ and $3d$ calculation in our two-band calculations as MgB_2 has a $2d$ σ-band and a $3d$ π-band, and there is a overall factor of 2/3 between the two in the nonlinear term due to dimensionality.

To obtain the nonlinear current as $q_s \to 0$, the general expression for the current can be expanded to second lowest order in powers of q_s leading to the general formula

$$j_s = j_0\left[A\left(\frac{q_s v_F^*}{\Delta_0}\right) - B\left(\frac{q_s v_F^*}{\Delta_0}\right)^3\right], \tag{5}$$

where only first and third order terms arise. Here by choice $j_0=ne\Delta_0/(mv_F)$ and the variable for the expansion was taken as $q_s v_F^*/\Delta_0$, where $v_F^*=v_F/(1+\lambda)$. A and B are temperature-dependent coefficients which follow when solutions of the Eliashberg equations (2) and (3) are substituted in the expression (1) for the current. In practice, it is complicated to expand Eqs. (1)–(3) to obtain an explicit form B and so we choose to extract A and B numerically by solving our full set of equations with no approximations for j_s versus q_s. From this numerical data, we find the intercept and slope of j_s/q_s versus q_s^2 for $q_s \to 0$ from which we obtain the A and B, respectively.

The results for $A(T)$ and $B(T)$ as a function of temperature are shown in Fig. 2. One sees, in the inset, $A(T)$ which, in the one-band case, is just the superfluid density n_s normalized to the clean BCS value at $T=0$. There is no difference between $2d$ and $3d$ BCS. Also, shown is the $A(T)$ extracted for the strong electron-phonon coupling superconductor Pb with no impurities and with impurity scattering of $t^+=T_{c0}$. One sees

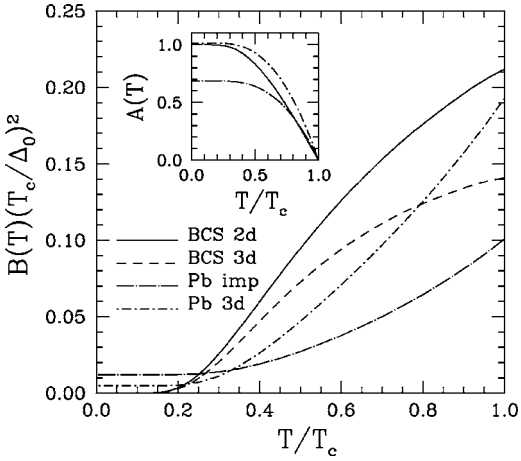

FIG. 2. The nonlinear coefficient $B(T)$ defined in Eq. (5) multiplied by $(T_c/\Delta_0)^2$ as a function of T/T_c. The solid curve is for $2d$ BCS, while the dashed is for $3d$ BCS. The dotted-short-dashed curve is for Pb in $3d$, which has been evaluated within Eliashberg theory, and the dotted-long-dashed curve shows the effect of impurities on Pb, where $t^+=T_{c0}$. The inset shows the temperature dependence of the linear coefficient $A(T)$ of Eq. (5), which is proportional to the superfluid density.

that strong coupling pushes the temperature dependence of the curve higher, even slightly so at $T=0$, and this is a well-documented effect.[28] With impurities, the superfluid density is reduced in accordance with standard theory. These curves were obtained from our j_s calculations and agree exactly with BCS and Eliashberg calculations done with the standard penetration depth formulas,[28] confirming that our numerical procedure is accurate. The second term in Eq. (5) gives the nonlinear current and the coefficient $B(T)$, which is a measure of this, is also shown for the four cases. [Note that $B(T)$ is the same as the $\beta(T)$ of Ref. 6 for the one-band case.] Here one does find a difference between the $2d$ and $3d$ BCS curves showing that dimensionality can affect the nonlinear current. In the case of strong coupling one finds an increase in the nonlinear piece near T_c and also a finite contribution at low T which is unexpected in the usual BCS scenario. Impurities have the effect of further increasing the low T contribution and reducing the curve near T_c.

Near T equal to T_c ($t \equiv T/T_c$) in BCS, it can be shown analytically that

$$A = 2(1-t) \tag{6}$$

and for $3d$,

$$B = \frac{7}{6}\frac{\zeta(3)}{(\pi T_c)^2}\Delta_0^2 \tag{7}$$

as obtained in our previous paper, Ref. 26. The value of B for $2d$ is increased by a factor of 3/2. These numbers agree with the numerical calculations in Fig. 2, where the $3d$ BCS curve goes to 0.21 for $2d$ and 0.14 in $3d$.

There are two definitions in the literature for the nonlinear coefficient: one is denoted as $\alpha(T)$ due to Xu *et al.*[2] and the other, $b(T)$, used by Dahm and Scalapino,[13] is the one that is

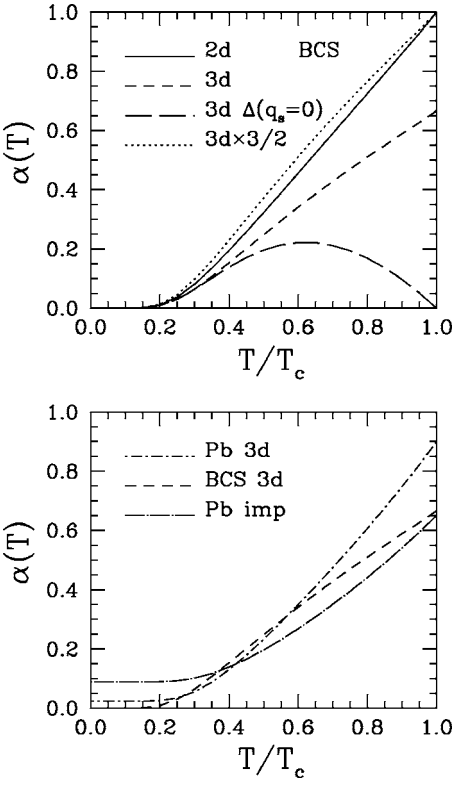

FIG. 3. The nonlinear coefficient $\alpha(T)$ defined in Xu, Yip, and Sauls (Ref. 2) [Eq. (10)] versus T/T_c. In the top frame, we show curves for $2d$ and $3d$ BCS. Multiplying the $3d$ BCS curve by 3/2 gives the dotted curve. The long-dashed curve illustrates, for the $3d$ case, the effect of not including the q_s-dependence in the gap equations. In the bottom frame, the strong-coupling Eliashberg theory result for Pb is shown, with the $3d$ BCS curve repeated for reference. The dotted-short-dashed curve is for pure Pb and the dotted-long-dashed is for $t^+=T_{c0}$.

related to the intermodulation power in microstrip resonators. Rewriting Eq. (5) in the form

$$j_s = j_0\left(\frac{q_s v_F^*}{\Delta_0}\right)A\left[1-\frac{B}{A^3}\left(\frac{j_s}{j_0}\right)^2\right], \tag{8}$$

Dahm and Scalapino define[13]

$$b(T) \equiv \frac{B}{A^3}. \tag{9}$$

Xu, Yip, and Sauls[2] keep the form of Eq. (5) but define a variable $q_s v_F^*/\Delta_0(T)$, where $\Delta_0(T)$ is the temperature dependent gap equal to $\Delta_0\delta(t)$. With this they identify the coefficient

$$\alpha(T) \equiv \frac{B}{A}\delta^2(t). \tag{10}$$

In this work, we always take $\delta(t)$ to be the usual BCS temperature dependence of the gap function.

In Fig. 3, we show the calculations for the $\alpha(T)$ coefficient of Xu *et al.* Here, we have made a number of points. First, the $2d$ BCS curve derived from our procedure agrees with that shown by Xu *et al.*,[2] once again validating our numerical work for extracting the very tiny nonlinear coefficient. Second, for BCS one sees a difference between $2d$ and $3d$ in the nonlinear coefficient. The $2d$ curve goes to 1 at T_c and to 2/3 for the $3d$ case. The question arises as to whether the difference between $2d$ and $3d$ is simply a numerical factor and so with the dotted curve, we show the $3d$ case scaled up by 3/2. We do note that there is a small difference in the temperature variations at an intermediate range of T, but the major difference between $2d$ and $3d$ is the overall numerical factor of 2/3. Third, one might question the necessity of including the effect of the current on the gap itself and to answer this, we show the long-dashed curve where the q_s dependence was omitted in the Eliashberg equations (2) and (3). One finds that the nonlinear coefficient is reduced substantially at temperatures above $\sim 0.5T_c$ and disappears at T_c. Thus, without the q_s dependence in the gap, the true nonlinear effects will not be obtained for high temperatures as the gap provides the major contribution to the nonlinearity.

In the lower frame of Fig. 3, we examine the case of Pb to illustrate strong electron-phonon coupling and impurity effects. It is seen that the strong coupling increases the value at T_c and also gives a finite value at low T. The behavior at low T is surprising in light of the BCS result,[2] but is related to the inelastic electron-phonon scattering which appears to increase the nonlinear coefficient at small T in a similar way to what is already known about the effect of impurities in BCS.[13] The strong-coupling behavior near T_c is similar to that seen for other quantities such as the specific heat,[28] where the downward BCS curvature is now turned concave upward to higher values at T_c. Impurities have the effect of reducing the nonlinearity near T_c and increasing it at low T.

Once again, in BCS we can provide some analytic results near and at T_c for $\alpha(t)$ which provide a useful check on our numerical work. For three dimensions near T_c,

$$\alpha(t) = \frac{7\zeta(3)}{12\pi^2}\left(\frac{\Delta_0}{T_c}\right)^2\frac{\delta^2(t)}{1-t} \tag{11}$$

and, upon substituting for $\delta(t)$,

$$\alpha(t=1) = \tfrac{2}{3}. \tag{12}$$

Doing the same algebra for the two-dimensional case corrects these expressions by a factor of 3/2 and gives 1 instead of 2/3 for $\alpha(t=1)$.

To characterize the strong-coupling effects seen in the figure for Pb, we can develop a strong-coupling correction formula for $\alpha(t=0)$ and $\alpha(t=1)$. These formulas have been provided in the past for many quantities and form a useful tool for experimentalists and others to estimate the strong-coupling corrections.[28] This was done by evaluating this quantity for 10 superconductors using their known $\alpha^2F(\omega)$ spectra and their T_c values. We used Al, V, Sn, In, Nb, V_3Ga, Nb_3Ge, Pb, $Pb_{0.8}Bi_{0.2}$, and $Pb_{0.65}Bi_{0.35}$. These materials were chosen to span the range of typical s-wave superconductors with strong-coupling parameter $T_c/\omega_{\ln}$ ranging from 0.004 to 0.2. The details of these materials and references for the spectra may be found in the review by Carbotte.[28] The parameter $\omega_{\ln}$ is defined as

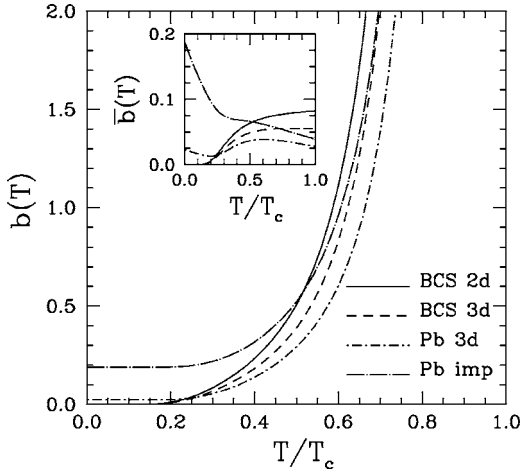

FIG. 4. The temperature dependence of the nonlinear coefficient $b(T)$ defined by Dahm and Scalapino (Ref. 13) [Eq. (9)] versus T/T_c. Shown are results for $2d$ and $3d$ BCS (solid and dashed curves, respectively) and $3d$ Pb in Eliashberg theory (dotted-short-dashed). As before these curves are for the pure case and one impure case for Pb is shown (dotted-long-dashed curve) with $t^+=T_{c0}$. The inset shows $\bar{b}(T)$ versus T/T_c, which is defined in Eq. (16).

$$\omega_{\ln} = \exp\left(\frac{2}{\lambda}\int_0^\infty \ln(\omega)\frac{\alpha^2 F(\omega)}{\omega}d\omega\right). \tag{13}$$

By fitting to these materials, we arrived at the following strong-coupling correction formulas for three dimensions:

$$\alpha(T_c) = \frac{2}{3}\left[1 + 7.7\left(\frac{T_c}{\omega_{\ln}}\right)^2 \ln\left(\frac{3\omega_{\ln}}{T_c}\right)\right] \tag{14}$$

and

$$\alpha(T=0) = 1.6\left(\frac{T_c}{\omega_{\ln}}\right)^2. \tag{15}$$

Note that, even though $ax^2\ln(b/x)$ is the usual form of the strong-coupling correction, in this last equation, we have found no advantage in fitting with the additional parameter offered by the log factor. These formula should be seen as approximate tools to give the trend for $T_c/\omega_{\ln}$ for values restricted to the range of 0 to 0.2. Pb has $T_c/\omega_{\ln}$ value of 0.128 and is intermediate to this range, and Al is a weak-coupling superconductor with a value of 0.004.

In Fig. 4, we show the coefficient used by Dahm and Scalapino[13] for the same cases as previously considered. With this coefficient one finds qualitatively similar curves. The $2d$ and $3d$ BCS curves go to zero rapidly at low temperature, but once again the strong coupling effects in Pb give a finite value for $b(T)$ at low T. With impurities the tail at low temperature is raised significantly. Due to the divergence in $b(T)$ near T_c because of the division by three powers of the superfluid density which is going to zero at T_c, we prefer to work with a new quantity $\bar{b}(t)$, which removes this divergence. Thus, we define

$$\bar{b}(t) \equiv b(t)(1-t)^3 \tag{16}$$

and this is shown in the inset in Fig. 4. It has the advantage of illustrating the detailed differences between the curves more clearly and providing finite values at T_c which can be evaluated analytically in BCS theory. In this instance, we obtain

$$\lim_{t\to 1}\bar{b}(t) = \frac{7\zeta(3)}{48\pi^2}\left(\frac{\Delta_0}{T_c}\right)^2 = 0.0557 \tag{17}$$

for three dimensions in agreement with what we obtain from our numerical work, shown in Fig. 4. Once again we can develop strong-coupling formulas for this quantity and they are given as

$$\bar{b}(T_c) = 0.0557\left[1 - 42.8\left(\frac{T_c}{\omega_{\ln}}\right)^2 \ln\left(\frac{\omega_{\ln}}{3.8T_c}\right)\right] \tag{18}$$

and

$$\bar{b}(T=0) = b(T=0) = 1.4\left(\frac{T_c}{\omega_{\ln}}\right)^2 \tag{19}$$

for three dimensions. Once again, there was no extra advantage to fitting $\bar{b}(T=0)$ with the usual form that includes the log factor.

This last quantity $b(t)$ is related to the intermodulation power in microstrip resonators and hence can be measured directly. Having identified the features of one-band superconductors, we now turn to the two-band case where signatures of the two-band nature may occur in these nonlinear coefficients.

IV. TWO-BAND *s*-WAVE SUPERCONDUCTORS

The generalization of Eq. (8) to the two-band case proceeds as follows. The total current j_s is the sum of the two partial currents j_{si}, $i=1,2$ with $(1,2)\equiv(\sigma,\pi)$ for the two-dimensional σ- and three-dimensional π-band, respectively. For our numerical work, we do take into account the different dimensionality of the bands but, for simplicity in our analytic work below, we take them both to be three dimensional. A decision needs to be taken about the normalization of the current j_s in the second term. Dahm and Scalapino have used $j_{0\pi}=n_\pi e\Delta_{0\pi}/(mv_{F\pi})$. Here instead, we prefer to use the more symmetric form

$$j_{00} = \sum_{i=1}^{2} j_{0i} = \sum_{i=1}^{2}\frac{en_i\Delta_{0i}}{mv_{Fi}}, \tag{20}$$

which reduces properly to the one-band case when our two bands are taken to be identical, with $n_1=n_2=n/2$, where n is the total electron density per unit volume. For the combined system, Eqs. (9) and (10) still hold with A and B modified as follows:

$$A = \frac{1}{j_{00}}\left(\frac{1}{2}\sum_{i=1}^{2}\frac{v_{Fi}^*}{\Delta_{0i}}\right)^{-1}\sum_{i=1}^{2} j_{0i}A_i\frac{v_{Fi}^*}{\Delta_{0i}} \tag{21}$$

and

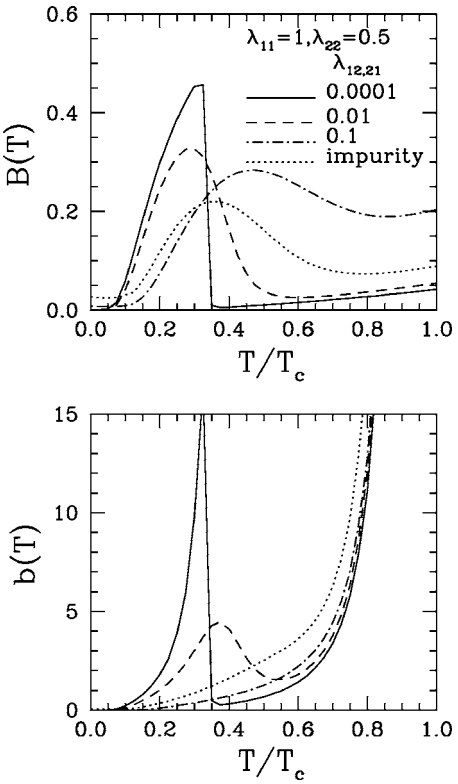

FIG. 5. The temperature dependence of nonlinear coefficient $B(T)$ (top frame) and $b(T)$ (bottom frame) for a model two-band superconductor based on a Lorentzian model for the spectral densities $\alpha_{ij}^2F(\omega)$, as described in the text. Shown is the effect of increased interband coupling, beginning with a nearly decoupled curve with $\lambda_{12}=\lambda_{21}=0.0001$ (solid) and progressing to more interband coupling with $\lambda_{12}=\lambda_{21}=0.01$ (dashed) and 0.1 (dotted-dashed). The dotted curve is for $\lambda_{12}=\lambda_{21}=0.0001$ and with interband impurity scattering of $t_{12}^+=t_{21}^+=0.1T_{c0}$ included.

$$B=\frac{1}{j_{00}}\left(\frac{1}{2}\sum_{i=1}^{2}\frac{v_{Fi}^*}{\Delta_{0i}}\right)^{-3}\sum_{i=1}^{2}j_{0i}B_i\left(\frac{v_{Fi}^*}{\Delta_{0i}}\right)^3. \tag{22}$$

With these definitions Eq. (5) also holds with j_{00} replacing j_0 and the Xu, Yip, and Sauls variable, $q_sv_F^*/\Delta_0(T)$, of the one-band case is replaced by $[q_s/2\delta(t)]\Sigma_{i=1}^2v_{Fi}^*/\Delta_{0i}$, with $\delta(t)$ the usual temperature profile of the BCS gap. Other choices could be made. The superfluid density n_s is proportional to A for the combined system, specifically en_s/m is given by Eq. (21) with the first two factors omitted.

In Fig. 5, we show both the $B(T)$ and the $b(T)$ for a model which uses truncated Lorentzians for the $\alpha^2F_{ij}(\omega)$ spectra. This same model was used in our previous work[10] and so we refer the reader to that paper for details. Also, in Ref. 10 may be found the curves for the $\Delta_i(T)$, the penetration depth, and other quantities for the same parameters used here. The essential parameters of this model are $\lambda_{11}=1$, $\lambda_{22}=0.5$ and the interband electron-phonon coupling is varied from $\lambda_{12}=\lambda_{21}=0.0001$ (nearly decoupled case) to 0.1 (more integrated case). In addition, the $\mu_{ij}^*=0$, $v_{F1}=v_{F2}$, and $n_1=n_2$. In the nearly decoupled case of $\lambda_{12}=\lambda_{21}=0.0001$, it can be seen that the solid curve looks like a superposition of two separate superconductors, one with a T_c which is about 0.33 of the bulk T_c. The lower temperature part of this curve is primarily due to the π-band (or band 2) which is three dimensional, and indeed, when examined in detail, it has the characteristic behavior of the $3d$ example studied in the one-band case. The part of the curve at higher temperatures above about $t\sim0.35$ is due to the σ-band (or band 1) which is taken to be $2d$ and indeed, in the case of $B(T)$ it shows a dependence approaching T_c that is expected for $2d$ strong coupling with some interband effects. The relative scale of the two sections of the curve is set by the value of the gap anisotropy $u=\Delta_{02}/\Delta_{01}$ and the ratio $(1+\lambda_{11}+\lambda_{12})/(1+\lambda_{22}+\lambda_{21})$. The overall scale on the y axis for $b(T)$ differs from that of Fig. 4 due to our choice of j_{00} for the normalization in the nonlinear term. Indeed, for nearly decoupled bands (solid curve), the value of the nonlinear coefficient $b(T)$ is small at reduced temperature $t=0.4$ just above the sharp peak due to band 2. Specifically, it is of order 0.5. If it had been referred to $j_{0\sigma}$ instead of j_{00}, it would be smaller still by a factor of 1.7 and comparable to the single band $2d$ BCS result at the same reduced temperature (Fig. 4 bottom frame, solid curve). However, as the nondiagonal electron-phonon couplings λ_{12} and λ_{21} are increased and a better integration of two bands proceeds, $b(T)$ at $t=0.4$ can increase by an order of magnitude as, for example, in the dashed curve. The actual scale in this region is set by the details of the electron-phonon coupling (see later the specific case of MgB_2).

With more integration between the bands, one finds that the sharp peak at lower T is reduced and rounded with a tail reaching to T_c. When $\lambda_{12}=\lambda_{21}=0.1$, the feature characteristic of the π-band T_c is almost gone in $B(T)$ and absent entirely in $b(T)$, even for modest interband coupling. The same conclusion holds for the effects of interband scattering (shown in Fig. 5 for a value of $t_{12}^+=t_{21}^+=0.1T_{c0}$ for the nearly decoupled case) which also integrates the bands and eliminates the lower energy scale. However, while the structure at the lower T_c is now reduced to the point of giving a monotonic curve for $b(T)$, there still remains a large nonlinear contribution well above that for the one-band s-wave case, which marks the presence of the second band.

We can have further insight into these results and check our work by developing some simple analytic results in renormalized BCS theory (RBCS). For a summary of the approximations of RBCS and a comparison with full numerical solution for various properties including j_s, we refer the reader to our previous work.[10,26] For simplicity, we take both bands to be three dimensional in the following. Near $T=T_c$, Eqs. (6) and (7) are modified for each band to

$$A_i=2(1-t)\frac{1}{\chi_i} \tag{23}$$

and

$$B_i=\frac{7}{6}\frac{\zeta(3)}{(\pi T_c)^2}\frac{\Delta_{0i}^2}{\chi_i'}, \tag{24}$$

where the functions χ_i and χ_i' have been derived in Ref. 26 and $v_{Fi}^{*2}\chi_i'$ is independent of v_{Fi}^*, where $v_{Fi}^*=v_{Fi}/(1+\Sigma_j\lambda_{ij})$. The χ's depend on the microscopic parameters of the theory.

In RBCS, they are λ_{ij}, μ^*_{ij}, v_{Fi}, and n_i, from which T_c and Δ_{0i} follow. While the expressions obtained for the χ_i and χ_i' are lengthy, and hence we do not repeat them here, they are explicit algebraic forms. It is useful in this work to consider several simplifying limits. For decoupled bands $\lambda_{12}=\lambda_{21}=\mu^*_{12}=\mu^*_{21}=0$ and $A_2=B_2=0$. As the band 2 does not contribute near T_c, A_1 and B_1 take on the form of the single band case [Eqs. (6) and (7)]. Another limiting case is the separable anisotropy model.[26] In this model, there are only two gap values with a ratio of $u=(1-a)/(1+a)$, with a an anisotropy parameter often assumed small. In this case, $\bar{\lambda}_{11}=\bar{\lambda}(1+a)^2/2$, $\bar{\lambda}_{22}=\bar{\lambda}(1-a)^2/2$, and $\bar{\lambda}_{12}=\bar{\lambda}_{21}=\bar{\lambda}(1-a^2)/2$, where $\bar{\lambda}=\lambda/(1+\lambda)$ and $\bar{\lambda}_{ij}=\lambda_{ij}/(1+\Sigma_l\lambda_{il})$. As a result

$$\frac{1}{\chi_1}=(1+a)^2(1-5a^2), \quad \frac{1}{\chi_2}=(1-a)^2(1-5a^2), \quad (25)$$

and

$$\frac{1}{\chi_i'}=\frac{v_{Fi}^{*2}}{\chi_i}. \quad (26)$$

In this model, taking in addition that $v_{F1}=v_{F2}$ and $n_1=n_2=n/2$ leads to the one-band case and this can be used as a check of our algebra.

To see the consequences of this algebra for our nonlinear coefficient $b(T)$, we begin with the decoupled band case near $T=T_c$ for which $A_2=B_2=0$ and A_1 and B_1 reduce to their single band value. In this limit of $t\to 1$,

$$b(t)=\frac{B_1}{A_1^3}\left(1+u\frac{v_{F1}}{v_{F2}}\right)^2, \quad (27)$$

where u is the gap anisotropy parameter $u=\Delta_{02}/\Delta_{01}$, and Δ_{0i} is the gap at $T=0$. This expression shows explicitly the corrections introduced by the two-band nature of the system over the pure one-band case. Note that $b(T)$ is always increased by the presence of the correction term. In (27), u can never be taken to be one since we have assumed band 2 is weaker than band 1. Before leaving the decoupled case, it is worth noting that $b(T)$ will show a change at the band 2 critical temperature T_{c2}. For T below T_{c2}, A_2 and B_2 will be finite while above this temperature they are both zero. When the coupling λ_{12} and λ_{21} is switched on but still small, we expect that these quantities will acquire small tails and that they vanish only at T_c. This is the hallmark of nearly decoupled bands.

For the anisotropic a^2 model near T_c,

$$b(t)=\frac{7\zeta(3)}{6\pi^2}\left(\frac{\Delta_0^{\rm av}}{T_c}\right)^2\frac{1+8a^2}{[2(1-t)]^3}, \quad (28)$$

where the average gap $\Delta_0^{\rm av}$ is related to T_c by $2\Delta_0^{\rm av}/T_c=3.54(1-3a^2/2)$. For $a^2=0$ this expression reduces properly to the one-band limit. Therefore, it is seen that anisotropy increases $b(T)$ for T near T_c.

Another interesting limiting case is to assume both bands are the same, i.e., isotropic gap case, but that the Fermi velocities differ in the two bands. Near T_c, we obtain

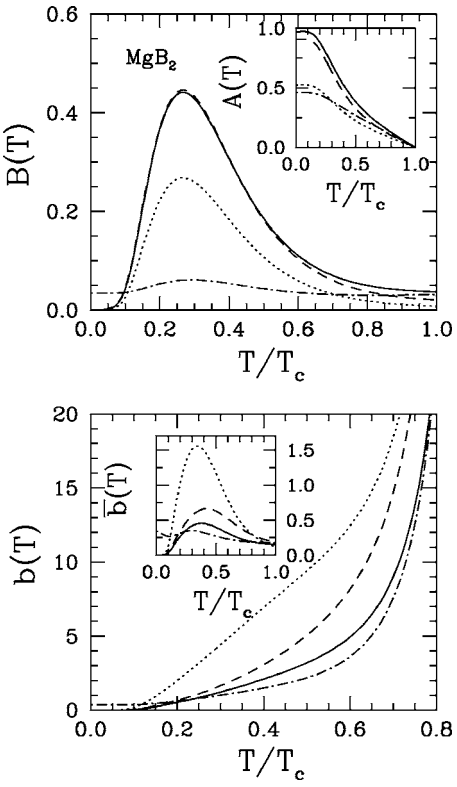

FIG. 6. The nonlinear coefficients $B(T)$ (top frame) and $b(T)$ (bottom frame) versus T/T_c for the case of MgB_2. The solid curve is for the pure case (no impurity scattering), the dashed for impurities in the σ band with $t_{11}^+=T_{c0}$ and dotted-dashed for $t_{22}^+=T_{c0}$. In the pure case, increasing the ratio of $v_{F2}/v_{F1}=3$ gives the dotted curve. The inset in the top frame gives $A(T)$ vs T/T_c and the bottom frame inset shows $\bar{b}(T)$.

$$b(t)=\frac{7\zeta(3)}{6\pi^2}\left(\frac{\Delta_0}{T_c}\right)^2\frac{1}{[2(1-t)]^3}\frac{1}{8}\frac{(v_{F1}+v_{F2})^2}{(v_{F1}v_{F2})^2}(v_{F1}^2+v_{F2}^2). \quad (29)$$

In this case, the Fermi velocity anisotropy changes the nonlinear coefficient, but when $v_{F1}=v_{F2}$ the expression reduces properly to the one-band result. We find that the Fermi velocity anisotropy increases $b(T)$ near T_c, a result that is seen in one of our calculations for MgB_2 shown in Fig. 6.

With Fig. 6, we now turn to the specific case of MgB_2, where we have used the parameters and $\alpha^2F_{ij}(\omega)$ given by band structure calculations, and as a result, there are, in principle, no free parameters other than varying the impurity scattering rate. The basic parameters are $\lambda_{\sigma\sigma}=1.017$, $\lambda_{\pi\pi}=0.448$, $\lambda_{\sigma\pi}=0.213$, $\lambda_{\pi\sigma}=0.155$, $\mu^*_{\sigma\sigma}=0.210$, $\mu^*_{\pi\pi}=0.172$, $\mu^*_{\sigma\pi}=0.095$, $\mu^*_{\pi\sigma}=0.069$, with a $T_c=39.5$ K and a gap anisotropy of $u=0.37$. The ratio of the two density of states is $N_\pi(0)/N_\sigma(0)=1.37$ and of the Fermi velocities is $v_{F\pi}/v_{F\sigma}=1.2$. We have found excellent agreement between theory and experiment for these parameters, as have other authors.[10,26] As we have found in our previous work, MgB_2 is quite integrated between the bands. It is also an intermediate strong coupler with $T_c/\omega_{\ln}=0.05$ and thus there is competition between the strong-coupling effects and the two-

band anisotropy.[10] In Fig. 6, the solid curve gives the prediction for MgB_2 for $B(T)$ and $b(T)$. A strong nonmonotonic feature around the lower band energy scale is observed in $B(T)$, but the $b(T)$ is monotonically increasing with temperature. To see the second band effects in $b(T)$, it is better to plot $\bar{b}(T)$ (the inset) which accentuates the subtle variations found at the lower energy scale associated with the π band. Also shown in the inset for the upper frame is $A(T)$, which gives the temperature dependence of the superfluid density. The solid curve agrees with our previous calculation by other means.[10] The variation in $A(T)$ appears to be sufficient to remove the bump in $B(T)$ when divided by three factors of $A(T)$ to obtain the definition of $b(T)$. Also, shown are the effects of intraband scattering with $t_{11}^{+}=T_{c0}$ for the dashed curve and $t_{22}^{+}=T_{c0}$ for the dotted-dashed curve. Scattering in the π-band reduces its contribution and provides an impurity tail at low T, as found for the one-band case. However, scattering in the σ-band, while lowering $B(T)$ near T_c as expected, does not appear to add weight at low T. This is because the parameters for MgB_2 heavily weight the π-band and the σ-band is a small component. Thus, upon comparison between σ- and π-band scattering, $b(T)$ could be lowered at $t=0.5$, for example, by putting impurities in the π-band, but it would be raised if the impurity scattering is in the σ-band. The dotted curve in the figure is for pure MgB_2 but where we have taken $v_{F2}/v_{F1}=3$ to mimic a case where transport may happen along the c axis. In this instance, the bump in $B(T)$ remains, but is gone in $b(T)$. We see that $b(T)$ is large due to the higher power of the Fermi velocity ratio that enters the calculation, and, as a result, the nonlinearity is greatly increased. As $b(T)$ is a relevant quantity for microwave filter design, this study provides some insight into which factors may be used to optimize the material and reduce the nonlinear effects.

V. CONCLUSIONS

Study of nonlinear current response is important for device applications and for providing fundamental signatures of order parameter symmetry, such as have been examined in the case of d-wave superconductivity. In this paper, we have considered the case of two-band superconductors. In so doing, we also reexamined the one-band case and discovered that there can exist extra nonlinearity at both low and high temperatures due to strong electron-phonon coupling, for which we have provided strong-coupling correction formulas, whereas the excess nonlinearity induced by impurity scattering occurs primarily at low temperatures. At T_c, impurities will give an enhanced or decreased contribution depending on the particular nonlinear coefficient discussed. In this paper, we have examined two nonlinear coefficients defined in the literature, one due to Xu *et al.*[2] and one defined by Dahm and Scalapino, with an emphasis on the latter as it is related to the intermodulation power in microstrip resonators.[13]

We have also studied issues associated with dimensionality motivated by the two-band superconductor MgB_2, which has a two-dimensional σ-band and a three-dimensional π-band. Within our one-band calculation, aside from an overall factor of 2/3, we find little difference in the temperature variation of the nonlinear coefficient in mean-field between $2d$ and $3d$. This is further reduced by strong-coupling effects.

For two-band superconductors, we show that for nearly decoupled bands a strong signature of the small gap π-band will appear in the nonlinear coefficients, but with increased interband coupling or interband scattering, such a signature will rapidly disappear. Likewise, intraband impurities in the π-band will wash out the temperature variation of the π-band, whereas the intraband impurities in the σ-band largely effect the nonlinearity at higher temperatures above the energy scale of the π-band, for the parameters typical to MgB_2.

We provide a prediction for the nonlinear coefficient in MgB_2 using the parameters set by band structure calculations. As the bands in MgB_2 are quite integrated, we find that the nonlinear coefficient $b(T)$ is monotonically increasing in contrast to a previous prediction, which was based on a number of approximations,[13] and we find that the increased nonlinearity due to the π-band is best reduced at $t=0.5$ by adding impurities to the π-band. Should the supercurrent sample the c-axis direction, a larger value in the Fermi velocity ratio between the bands would result and this effect is found to increase the nonlinearity. Finally, several simple formulas have been provided for near T_c which aid in the understanding of the range of behavior observed in the numerical calculations. We await experimental verification of our predictions.

ACKNOWLEDGMENTS

The authors thank Dr. Ove Jepsen for supplying the MgB_2 electron-phonon spectral functions and one of the authors (D.J.S.) would like to acknowledge useful discussions with Dr. Thomas Dahm. This research was funded by NSERC (E.J.N. and J.P.C.), the Government of Ontario (PREA) and the University of Guelph (E.J.N.), the CIAR (J.P.C.), and NSF Grant No. DMR02-11166 (D.J.S.). In addition, support was provided in part by NSF Grant No. PHY99-07949 through the KITP, where this work was initiated.

*Electronic address: nicol@physics.uoguelph.ca
†Electronic address: carbotte@mcmaster.ca
‡Electronic address: djs@vulcan.physics.ucsb.edu

[1] S. K. Yip and J. A. Sauls, Phys. Rev. Lett. **69**, 2264 (1992); D. Xu, S. K. Yip, and J. A. Sauls, Physica B **94-196**, 1595 (1994).
[2] D. Xu, S. K. Yip, and J. A. Sauls, Phys. Rev. B **51**, 16233 (1995).
[3] A. Maeda, Y. Iino, T. Hanaguri, N. Motohira, K. Kishio, and T. Fukase, Phys. Rev. Lett. **74**, 1202 (1995); A. Maeda, T. Hanaguri, Y. Iino, S. Matsuoka, Y. Kokata, J. Shimoyama, K. Kishio, H. Asaoka, Y. Matsushita, M. Hasegawa, and H. Takei, J. Phys. Soc. Jpn. **65**, 3638 (1996); A. Bhattacharya, I. Zutić, O. T. Valls, A. M. Goldman, U. Welp, and B. Veal, Phys. Rev. Lett. **82**, 3132 (1999); A. Bhattacharya, I. Zutić, O. T. Valls, and A. M. Goldman, *ibid.* **83**, 887 (1999); C. P. Bidinosti, W. N. Hardy, D. A. Bonn, and R. Liang, *ibid.* **83**, 3277 (1999); A. Carrington, R. W. Giannetta, J. T. Kim, and J. Giapintzakis, Phys. Rev. B **59**, R14173 (1999).
[4] M. -R. Li, P. J. Hirschfeld, and P. Wölfle, Phys. Rev. Lett. **81**, 5640 (1998).
[5] Klaus Halterman, Oriol T. Valls, and Igor Žutić, Phys. Rev. B **63** 180405(R), (2001).
[6] T. Dahm and D. J. Scalapino, Phys. Rev. B **60**, 13125 (1999).
[7] D. E. Oates, S. H. Park, and G. Koren, Phys. Rev. Lett. **93**, 197001 (2004); J. C. Booth, J. A. Beall, D. A. Rudman, L. R. Vale, and R. H. Ono, J. Appl. Phys. **86**, 1020 (1999).
[8] James C. Booth, K. T. Leung, Sang Young Lee, J. H. Lee, B. Oh, H. N. Lee, and S. H. Moon, Supercond. Sci. Technol. **16**, 1518 (2003); G. Lamura, A. J. Purnell, L. F. Cohen, A. Andreone, F. Chiarella, E. Di Gennaro, and R. Vaglio, Appl. Phys. Lett. **82**, 4525 (2003).
[9] J. Nagamatsu, N. Nakagawa, T. Muranaka, Y. Zenitani, and J. Akimitsu, Nature (London) **410**, 63 (2001).
[10] E. J. Nicol and J. P. Carbotte, Phys. Rev. B **71**, 054501 (2005).
[11] For example, Yu. A. Nefyodev, A. M. Shuvaev, and M. R. Trunin, cond-mat/0509244 (unpublished); V. Guritanu, W. Goldacker, F. Bouquet, Y. Wang, R. Lortz, G. Goll, and A. Junod, Phys. Rev. B **70**, 184526 (2004); Etienne Boaknin, M. A. Tanatar, Johnpierre Paglione, D. Hawthorn, F. Ronning, R. W. Hill, M. Sutherland, Louis Taillefer, Jeff Sonier, S. M. Hayden, and J. W. Brill, Phys. Rev. Lett. **90**, 117003 (2003).
[12] For example M. A. Tanatar, Johnpierre Paglione, S. Nakatsuji, D. G. Hawthorn, E. Boaknin, R. W. Hill, F. Ronning, M. Sutherland, Louis Taillefer, C. Petrovic, P. C. Canfield, and Z. Fisk, Phys. Rev. Lett. **95**, 067002 (2005); P. M. C. Rourke, M. A. Tanatar, C. S. Turel, J. Berdeklis, J. Y. T. Wei, and C. Petrovic, *ibid.* **94**, 107005 (2005).
[13] T. Dahm and D. J. Scalapino, Appl. Phys. Lett. **85**, 4436 (2004).
[14] A. A. Golubov, J. Kortus, O. V. Dolgov, O. Jepsen, Y. Kong, O. K. Andersen, B. J. Gibson, K. Ahn, and R. K. Kremer, J. Phys.: Condens. Matter **14**, 1353 (2002).
[15] K. T. Rogers, Ph.D. thesis, University of Illinois, 1960 (unpublished).
[16] J. Bardeen, Rev. Mod. Phys. **34**, 667 (1962).
[17] R. H. Parameter, RCA Rev. **23**, 323 (1962); R. H. Parameter, and L. J. Berton, *ibid.* **25**, 596 (1964).
[18] K. Maki, Prog. Theor. Phys. **29**, 10 (1963); **29**, 333 (1963).
[19] K. Maki, in *Superconductivity*, edited by R. D. Parks (Dekker, New York, 1969), p. 1035.
[20] M. Y. Kupriyanov and V. F. Lukichev, Sov. J. Low Temp. Phys. **6**, 210 (1980).
[21] T. R. Lemberger and L. Coffey, Phys. Rev. B **38**, 7058 (1988).
[22] E. J. Nicol and J. P. Carbotte, Phys. Rev. B **43**, 10210 (1991).
[23] D. Zhang, C. S. Ting, and C. -R. Hu, Phys. Rev. B **70**, 172508 (2004).
[24] I. Khavkine, H. Y. Kee, and K. Maki, Phys. Rev. B **70**, 184521 (2004).
[25] H. Y. Kee, Y. B. Kim, and K. Maki, Phys. Rev. B **70**, 052505 (2004).
[26] E. J. Nicol and J. P. Carbotte, Phys. Rev. B **72**, 014520 (2005).
[27] A. E. Koshelev and A. A. Golubov, Phys. Rev. Lett. **92**, 107008 (2004).
[28] J. P. Carbotte, Rev. Mod. Phys. **62**, 1027 (1990).